Appl. Phys. B 69, 505–507 (1999) / Digital Object Identifier (DOI) 10.1007/s003409900147

Applied Physics B
Lasers
and Optics

Rapid communication

Planar laser-induced fluorescence imaging of carbon monoxide using vibrational (infrared) transitions

B.J. Kirby*, R.K. Hanson

Mechanical Engineering Department, Stanford University, Stanford, CA 94305-3032, USA
(Fax: +1-650/723-1748, E-mail: bkirby@navier.stanford.edu)

Received: 30 July 1999/Published online: 16 September 1999

Abstract. We report a new imaging diagnostic suitable for measurements of infrared-active molecules, namely infrared planar laser-induced fluorescence (IR PLIF), in which a tunable infrared source is used to excite vibrational transitions in molecules and vibrational fluorescence is collected by an infrared camera. A nanosecond-pulse Nd:YAG-pumped KTP/KTA OPO/OPA system is used to generate 12 mJ of tunable output near 2.35 μm which excites the 2ν band of carbon monoxide (CO); fluorescence resulting from excited CO is collected at 4.7 μm by using an InSb focal plane array. Quantitative, high-SNR PLIF imaging of gas-phase CO is demonstrated at a 10-Hz acquisition rate with a minimum detection limit of 1350 ppm at 300 K.

PACS: 32.50.+d; 34.50.Ez; 39.30.+w

Infrared imaging diagnostics have undergone rapid expansion in recent years, due primarily to improved performance of infrared focal plane arrays (FPAs). Improved FPAs, combined with more robust infrared nonlinear optical crystals and low-divergence pulsed pump lasers, have made it possible to consider extending planar laser-induced fluorescence (PLIF) imaging diagnostics to the infrared. While PLIF imaging is well established as a diagnostic technique in which ultraviolet or visible photons are used to excite electronic transitions [1], many key species exist which lack suitable imaging diagnostics because their electronic transitions lie in the vacuum ultraviolet and therefore cannot be used for single-photon PLIF techniques. These species include, but are not limited to, important combustion species such as CO, H_2O, and CO_2.

Competing diagnostics for imaging species without convenient UV transitions include Raman scattering [2] and multi-photon PLIF techniques [3]. IR PLIF is a linear technique which offers higher signal levels than Raman scattering does (greater than 10^5 photons/pixel in this work). Linearity eases interpretation of data and increases quantitative accuracy, while high signal levels imply high SNR and large dynamic range. In this paper we present the IR PLIF technique and initial imaging results for carbon monoxide/argon/air mixing processes.

* Corresponding author.

1 Experimental setup

The experimental setup used for imaging is shown in Figs. 1 and 2. The tunable laser source (Fig. 1) is a high-pulse-energy (> 20 mJ/pulse near 2.0 μm), nanosecond-pulse, 10-Hz, single-longitudinal-mode (400 MHz), KTP/KTA OPO-OPA system pumped by the output of a Nd:YAG laser. This system is based on a 532-nm-pumped, grating-tuned KTP oscillator (Continuum Mirage 3000). Selected KTP crystals have been replaced with KTA crystals to minimize idler absorption in the region beyond ∼ 3.5 μm [4]. Since high pulse energies are required for planar imaging techniques, the mid-infrared pulses from this system have been amplified (with roughly 6 dB of gain) with a 1064-nm-pumped KTA OPA. As is well known, optical parametric amplifiers [5] are attractive due to both their high conversion efficiency and their wide tuning range. These advantages, combined with the insensitivity of parametric gain to the spectral properties of the input beams and the avoidance of experimental problems common to laser amplifiers (e.g. parasitic oscillations) make parametric amplification preferred for our application.

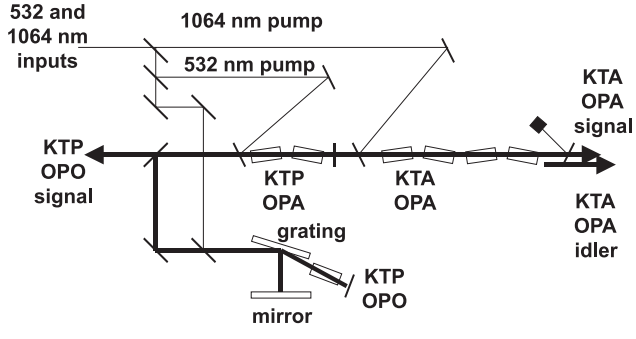

Fig. 1. Tunable infrared source consisting of modified Continuum Mirage 3000 OPO with KTA optical parametric amplifier stages added for increased conversion

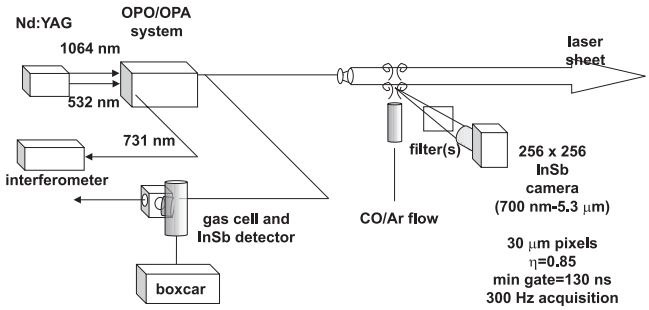

Fig. 2. Experimental setup for imaging experiments

The OPA system is tuned to 4288.28 cm^{-1} (Fig. 2) to pump the R(7) line of the 2ν band of CO at 2.35 μm. The near-infrared signal beam (731 nm) of the 532-nm-pumped OPO is monitored by using a commercial interferometer (Burleigh WA-4500) to ensure single-mode operation and to quantify the wavelength. The mid-infrared idler beam (2.35 μm) of the 1064-nm-pumped OPA is centered on the absorption line of interest through the use of a small CO test cell with CaF_2 windows for laser entry and fluorescence exit. OPA output is positioned spectrally by reflecting the OPA output into the cell and maximizing the resulting fluorescence recorded through a 4.7–5.1-μm filter by an InSb infrared detector (Judson J10D) and boxcar averager (SRS SR250). The beam is expanded vertically and focused horizontally by using fused silica cylindrical lenses to generate a sheet of height 4 cm and FWHM thickness 600 μm. The PLIF signal is collected through a 4.3–5.3-μm filter and an $f/2$ singlet CaF_2 lens at a magnification of 0.3 into a 256×256 InSb camera (Santa Barbara Focalplane SBF 134). The imaged region is roughly 2.5 cm × 2.5 cm in size and typical integration times range from 5 to 20 μs.

2 Imaging results and quantitative interpretation

A sample result (single-shot) is shown in Fig. 3. Representative peak signal-to-noise ratios for these images range from 150 to 200. The SNR of the images presented here can be used to infer a detection limit (SNR = 1) for the present experimental setup of 1350 ppm.

The fluorescence equation for PLIF imaging with weak excitation (no saturation effects) can be written as

$$S_\mathrm{f} = \frac{E}{h\nu} g S \ell \frac{P\chi_\mathrm{abs}}{kT} \phi \eta_\mathrm{c} \,, \tag{1}$$

where S_f is the fluorescence signal (photons per pixel); E (J) is the laser pulse energy incident on the imaged pixel volume; $h\nu$ (J) is the energy per photon; g (cm) is the convolution of the laser and absorption lineshapes; S (cm) is the line strength per number density, which takes into account the Boltzmann fraction of the absorbing species in the lower state of the laser transition; ℓ (cm) is the length of the area imaged onto the pixel; $P\chi_\mathrm{abs}/kT$ (cm^{-3}) is the number density of the species; ϕ is the fluorescence quantum yield; and η_c is the collection efficiency of the optics and camera. The parameters in (1) are well known from laser and camera properties as well as spectroscopic databases such as HITRAN [6], with the possible exception of the fluorescence quantum yield ϕ. Quantification of the fluorescence quantum yield requires modeling of state-specific energy transfer rates.

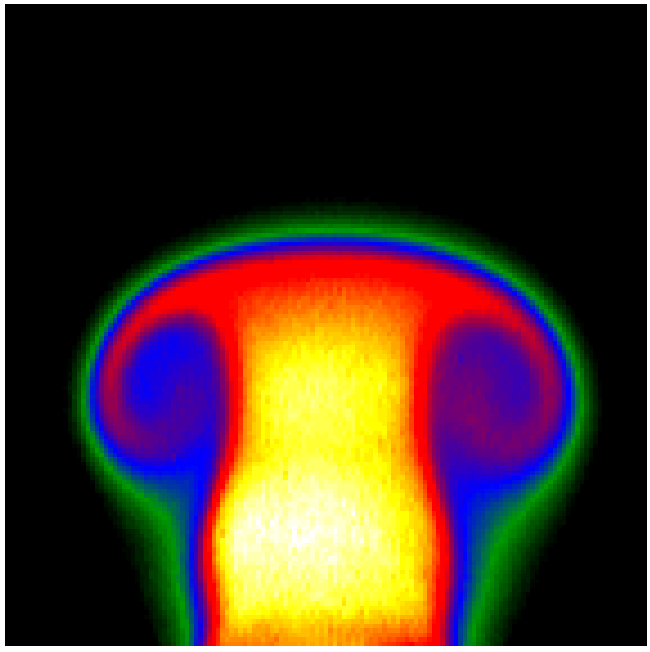

Fig. 3. Single-shot IR PLIF image of a vortex ring developing from a 6-mm tube. The jet fluid is 50% CO/50% Ar. The ambient gas is air. 12 mJ at 2.35 μm is used to excite the CO. The integration time is 20 μs

In general, the fluorescence quantum yield ϕ may be written as

$$\phi = \sum_j \int_0^\tau A_j \frac{n_j(t)}{N} \mathrm{d}t \,, \tag{2}$$

where the fluorescence is summed over j excited states. A_j is the Einstein A coefficient for the state j given a specific collection channel (e.g., $\Delta v = 1$); n_j is the instantaneous population in the excited state; N is the total number of absorbed laser photons; τ is the camera integration time. Emitting states are depleted by both radiative (A) and nonradiative (Q) processes which cause molecular transitions to states which do not emit within the collection bandwidth.

Equation (2) takes on simple forms in certain limits. For electronic transitions, typically $\tau \gg 1/(A+Q)$ and $Q \gg A$, causing (2) to reduce to the familiar $\phi = A/Q$. In contrast, for vibrational transitions and our camera system the camera integration time is shorter than, or comparable to, the fluorescence decay time, so $\phi \propto A\tau$. For quantitative accuracy, of course, (2) must be integrated as a function of the collision partners, temperature, pressure, and integration time. For the flow examined here (large CO mole fraction), near-resonant CO-CO vibration-to-vibration V-V transfer quickly removes CO molecules from the $v = 2$ state and populates the $v = 1$ state; this is followed by decay due to CO-N_2 (V-V) transfer. For short integration times, then, $A = A_1 \approx 35\ \mathrm{s}^{-1}$ and $\phi \approx 2A_1\tau$ for which a typical value is 2×10^{-4}. Pertinent vibrational transfer mechanisms for CO imaging in $CO/N_2/O_2/Ar$ systems are summarized in Table 1. These energy transfer processes are shown schematically in Fig. 4.

Table 1. Vibrational transfer mechanisms relevant to fluorescence quantum yield for CO Infrared PLIF [7, 8]

V-V Processes	$k(\mathrm{s}^{-1}\mathrm{bar}^{-1})$ at 300 K
$CO(2)+CO(0) \rightarrow CO(1)+CO(1)$	7.6×10^{7}
$CO(2)+N_2(0) \rightarrow CO(1)+N_2(1)$	5.4×10^{5}
$CO(1)+N_2(0) \rightarrow CO(0)+N_2(1)$	2.7×10^{5}

V-V energy transfer with oxygen, and all V-T (vibration-to-translation) processes, are negligible on the time scales relevant here.

In order to demonstrate the technique for quantitative interpretation of IR PLIF signals, a turbulent CO/Ar jet in a $CO/Ar/N_2$ coflow was imaged from x/D of 0 to 10. The same excitation and collection scheme used to generate Fig. 3 was employed with a nominal pulse energy of 12 mJ. Since the CO concentration in the coflow was known, the images are essentially self-calibrating. Post-processing steps are as follows: the PLIF signal in the coflow is fixed to the known coflow mole fraction, thereby calibrating the collection optics and correcting for sheet intensity variations; the laser attenuation is corrected for by using known absorption cross-sections; and a comprehensive model of fluorescence quantum yield is used to adjust for the (relatively minor) fluorescence quantum yield variations. A sample result is shown in Fig. 5. For these images, the 2-mm-diameter central jet (Re = 2800) consisted of 50% CO and 50% Ar, while the weak coflow consisted of 1.7% CO, 1.7% Ar, and 96.6% N_2. The signal level in this image is quantitatively related to the CO mole fraction as given by the color table. Values of the CO mole fraction in the potential core are reasonably constant and match the expected value of 50%. In addition, averaged cuts as the jet approaches the far-field regime ($x/D = 8$ is shown in the figure) agree with the expected Gaussian profile and FWHM far-field spreading rates for a turbulent jet.

3 Conclusions

We have introduced an infrared planar laser-induced fluorescence technique which is suitable for instantaneous 2D measurements of infrared-active molecules. We employed a nanosecond-pulse Nd:YAG-pumped KTP/KTA OPO/OPA system to generate high-energy pulses at 2.35 μm for excitation of carbon monoxide, with ensuing fluorescence collected at 4.7 μm by an InSb focal plane array. Quantitative, high-SNR IR PLIF imaging of gas-phase carbon monoxide at a 10-Hz acquisition rate has been demonstrated with a minimum detection limit at room temperature of 1350 ppm. Given that our OPO/OPA system provides output ranging from 1.3 to 4.7 μm, opportunity exists to extend these measurements to other molecules such as CO_2, H_2O, and CH_4.

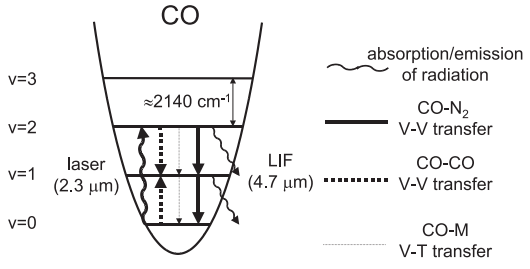

Fig. 4. Energy transfer diagram for CO molecules during CO LIF

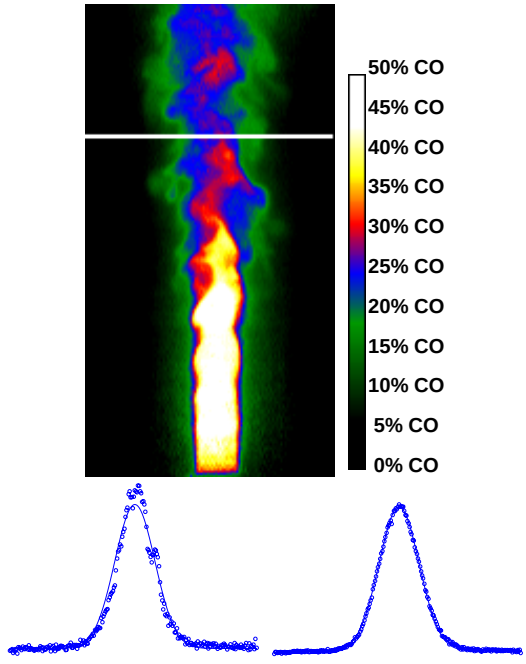

Fig. 5. Turbulent CO/Ar jet in $CO/Ar/N_2$ coflow. *Top*: Corrected single-shot instantaneous image. White line indicates $x/D = 8$. *Bottom*: normalized cuts at $x/D = 8$ for instantaneous (*left*) and averaged (*right*) images are shown in comparison with the gaussian curve which best fits the averaged data. Integration time is 5 μs

Acknowledgements. This research was supported by the Air Force Office of Scientific Research, Aerospace and Materials Sciences Directorate, with Dr. Julian Tishkoff as technical monitor.

References

1. J.M. Seitzman, R.K. Hanson: *Planar fluorescence imaging in gases*; In: A. Taylor (Ed.): Experimental Methods for Flows with Combustion, (Academic Press, London 1993)
2. M.B. Long, D.C. Fourguette, M.C. Escoda: Opt. Lett. **8**(5), 244 (1983)
3. J. Haumann, J.M. Seitzman, R.K. Hanson: Opt. Lett. **11**(**12**), 776 (1986)
4. W.R. Bosenberg, L.K. Cheng, J. D. Bierlein: Appl. Phys. Lett. **65**(22), 2765 (1994)
5. R.A. Baumgartner, R.L. Byer: IEEE J. Quant. Elect. **QE-15**(6), 432 (1979)
6. L.S. Rothman, C.P. Rinsland, A. Goldman, S.T. Massie, D.P. Edwards, J.M. Flaud, A. Perrin, C. Camy-Peyret, V. Dana, J.Y. Mandin, J. Schroeder, A. McCann, R.R. Gamache, R.B. Wattson, K. Yoshino, K.V. Chance, K.W. Jucks, L.R. Brown, V. Nemtchinov, P. Varanasi: J. Quant. Spectrosc. Radiat. Trans. **60**(5), 665 (1998)
7. M. Cacciatore, G. D. Billing: Chem. Phys. **58**(3), 395 (1981)
8. G. D. Billing: Chem. Phys. **50**(2), 165 (1980)